Original Research Article

Targeting EGFR Self-assembling RNA Nanoparticles Co-delivering Paclitaxel and miRNA21 Inhibitors for the Treatment of Head and Neck Tumors

Yuejuan Che[+,1,2,3,4], Zhuohao Wen[+,5], Jiali Shou[6], Yujuan Li[*,4], Miao Zhou[*,5], Chang Du[*,1,2,3]

[1]Department of Biomedical Engineering, School of Materials Science and Engineering, South China University of Technology, Guangzhou, 510641, China; *[2]National Engineering Research Center for Tissue Restoration and Reconstruction, South China University of Technology, Guangzhou, 510006, China; [3]China Key Laboratory of Biomedical Materials and Engineering of the Ministry of Education, and innovation Center for Tissue Restoration and Reconstruction, South China University of Technology, Guangzhou, 510006, China; [4]Department of Anesthesiology, Sun Yat-sen Memorial Hospital, Sun Yat-sen University, Guangzhou, 510120, China;[5]Department of Stomatology, Guangdong Provincial People's Hospital (Guangdong Academy of Medical Sciences), Southern Medical University, Guangzhou 510080, China;[6]Department of Ultrasound Medicine; Guangdong Provincial Key Laboratory of Major Obstetric Diseases; Guangdong Provincial Clinical Research Center for Obstetrics and Gynecology; The Third Affiliated Hospital, Guangzhou Medical University, Guangzhou, 510150, China*

ABSTRACT

Head and neck squamous cell carcinoma (HNSCC) primarily originate from epithelial tissues, with squamous cell carcinoma accounting for over 90% of cases. While surgery remains primary treatment approach, its outcomes are often unsatisfactory, underscoring the urgent need for innovative biological therapies to improve cure rates and survival. In this study, miRNA-mRNA interaction pairs with potential therapeutic were identified by data mining and bioinformatics techniques, considering miRNA expression profiles, regulatory networks, and target mRNA interactions. Human tongue squamous carcinoma cell line Cal27 was used as cell model, while RNA4WJ nanoparticles were employed as delivery vehicles to transport drug, nucleic acid aptamers, and therapeutic inhibitor for identified

ABBREVIATIONS: Figure note description, 4WJ: a four-stranded structured nucleic acid nanoparticle that may be used for vector-mediated drug delivery or specific gene expression regulation. EGFRapt: a ligand (aptamer) targeting the epidermal growth factor receptor (EGFR), indicating that this set of nanoparticles may have a function or effect that acts through the EGFR signaling pathway. LNA21: Locked Nucleic Acid 21 (LNA21) for miRNA targeting and regulation. PTX: paclitaxel, a commonly used anticancer drug for the treatment of a variety of malignant tumors.

***Please send correspondence to** Chang Du at cdu_gd@163.com (main corresponding author); Yuejuan Che at cheyj@mail.sysu.edu.cn; Miao Zhou at zhoumiao@gdph.org.cn.

Received February 24, 2025**; Accepted** July 3, 2025

[+]Yuejuan Che and Zhuohao Wen are both the co-first author of this study.

miRNA. Both *in vitro* and *in vivo* experiments demonstrated the precise delivery and selective inhibition of Cal27 cells, validated by the targeting and anticancer effects of RNA4WJ nanoparticles. Additionally, the underlying mechanisms of these therapeutic effects were explored. Collectively, this study provides a novel and promising therapeutic approach with significant potential for clinical application in HNSCC management.

Keywords: RNA nanotechnology; micro ribonucleic acids; head and neck squamous cell carcinoma; cancer therapy

INTRODUCTION

Head and neck squamous cell carcinoma (HNSCC), predominantly originating from epithelial tissues, represent a significant global health challenge. Among these, squamous cell carcinoma (SCC) constitutes the majority, characterized by high aggressiveness and rapid metastasis. Currently, head and neck squamous cell carcinoma (HNSCC) ranks as the sixth most common malignancy worldwide, with an increasing incidence rate annually[1, 2]. According to recent statistics, over 830,000 new cases of HNSCC are reported globally each year, resulting in more than 430,000 deaths, thereby imposing a considerable burden on healthcare systems[3]. While approximately 30-40% of patients are diagnosed at an early stage (stage I or II), which allows for interventions such as surgery and radiotherapy, over 60% of cases are identified at advanced stages (stage III or IV). Despite advances in medical technology and the development of comprehensive treatment modalities, the 5-year survival rate for HNSCC remains below 50%[4], highlighting the need for more effective therapeutic strategies to improve patient outcomes.

MicroRNAs (miRNAs) are small, non-coding RNAs that regulate gene expression post-transcriptionally by binding to the 3' untranslated regions (3' UTRs) of target mRNAs[5]. In HNSCC, miRNAs play dual roles as oncogenes or tumor suppressors, influencing key processes such as cell proliferation, apoptosis, invasion, and metastasis[6, 7]. Dysregulated miRNA expression is often associated with HNSCC development, progression, and resistance to therapy, making them potential biomarkers for diagnosis, prognosis, and therapeutic targets in HNSC[8]. However, the specific function and role of miR-21-5p in HNSCC remain unclear.

Nanotechnology presents a novel avenue for enhancing drug delivery by encapsulating therapeutic agents within nanocarriers, improving targeting, stability, and bioavailability. RNA nanotechnology, in particular, has gained attention for its ability to construct nanoparticles predominantly from RNA[9, 10]. These nanoparticles exhibit high thermal stability and can be engineered for precise delivery of therapeutic agents[11]. For instance, Guo *et al*. successfully developed pRNA-3WJ nanoparticles with exceptional thermodynamic stability, subsequently enhancing their resistance to ribonuclease (RNase) degradation through 2'-F modifications[12]. These RNA-3WJ motifs have been widely utilized as delivery platforms for cancer-specific therapies, demonstrating robust efficacy in preclinical models[13-17]. Building on this, RNA4WJ nanoparticles have been engineered to bind water-insoluble paclitaxel, increasing its solubility by over 32,000-fold and achieving efficient drug delivery[18]. Although RNA nanotechnology has shown significant potential in cancer therapy, its application in HNSCC remains unexplored.

This study aims to leverage bioinformatics and data mining technologies to identify miRNA-mRNA interaction pairs of therapeutic value, providing precise targeting options for personalized treatment of HNSCC (Fig. 1). Using human tongue squamous carcinoma cell line and xenograft models, the study will evaluate the targeting and antitumor effects of RNA4WJ nanoparticles carrying a conventional drug Paclitaxel (PTX), nucleic acid aptamer for epidermal growth factor receptor (EGFR) ligand, and therapeutic inhibitor for miR-21-5p. The findings will elucidate the underlying mechanisms of action and pave the way for innovative therapeutic approaches for clinical management of HNSCC.

MATERIALS AND METHODS

Ethic approval

This study was approved by the Ethics Committee on Animal Experiments of Guangzhou Medical University (Approval Number: GY2020-096).

Data Sources of miRNA and RNA-Seq

The miRNA-Seq isoform raw read counts and normalized RPM values, along with RNA-Seq raw read counts and normalized gene expression values (FPKM), for head and neck squamous cell carcinoma (HNSCC) were obtained from the TCGA-HNSCC (The Cancer Genome Atlas-Head and Neck Squamous Cell Carcinoma) dataset through the TCGA database (https://portal.gdc.cancer.gov/). Additionally, Gene Expression Omnibus (GEO), a public database providing extensive gene expression data, including miRNAs and mRNAs, was utilized. Two miRNA-Seq expression profiles datasets of HNSCC tissues, GSE28100 and GSE34496, were obtained from GEO.

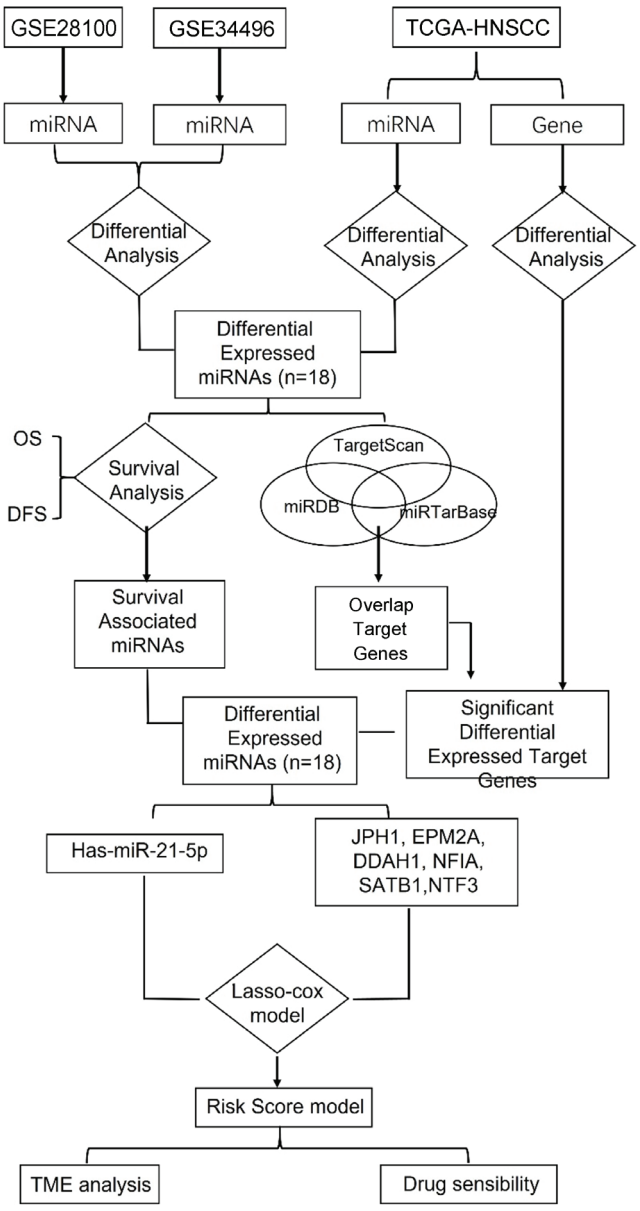

Fig. 1. Bioinformatics analysis flowchart. OS: overall survival; DFS: disease free survival; TME: tumor microenvironment.

The miRNA-Seq data from 34496 were downloaded and processed using the R package GEOquery This facilitated further exploration of miRNA expression profiles in HNSCC, enabling comparisons between the datasets to identify differential miRNA and RNA-Seq expression. Additionally, survival analyses, including disease-free survival (DFS) and overall survival (OS), were conducted to determine potential associations between miRNA expression and clinical outcomes.

Prediction of miRNA Target Genes

To reveal the mechanisms of action of the identified differential miRNAs in HNSCC, three established miRNA target prediction databases, including TargetScan, miRDB and miRTarBase, were used in this study. The predicted target genes from these databases were cross-referenced to identify a shared set of miRNA target genes. This approach aimed to determine potential miRNA targets specifically associated with HNSCC for further analysis.

Functional Analysis of Differentially Expressed miRNA Target Genes

To gain deeper insights into the roles of differentially expressed miRNA target genes in biological functions and metabolic pathways associated with HNSCC, functional enrichment analyses were conducted using R package clusterProfiler. This process includes Gene Ontology (GO), Kyoto Encyclopedia of Genes and Genomes (KEGG) pathway analysis, and Gene Set Enrichment Analysis (GSEA) of differentially expressed miRNA target genes. The aim of this analysis was to reveal the biological significance and key pathways involved in the development and progression of HNSCC.

Construction of a LASSO-COX Model Using miRNA and Target Gene Sets to Classify Risk Levels

To perform an in-depth analysis, target gene sets identified previously were further analyzed by extracting their FPKM values from the TCGA-HNSCC dataset, along with the relative miRNA expression levels (RPM). Using the R package glmnet, LASSO regression analysis was conducted to construct a multifactor Cox proportional hazards model for DFS, leading to the formulation of a risk score equation:

Risk score = $\beta_1 X_1 + \beta_2 X_2 + ... + \beta_n X_n$

Here, β represents the regression coefficient of each gene, while X represents the expression level of the corresponding gene. This risk score formula was applied to calculate the individual risk scores of patients, allowing for an assessment of their prognostic status in terms of DFS for HNSCC. A higher risk score indicates an elevated risk, whereas a lower score suggests a reduced risk.

Drug Sensitivity Analysis

The R package oncoPredict, designed for cancer drug sensitivity prediction and personalized treatment research, was utilized in this study. Its functionalities include drug sensitivity analysis and gene expression association analysis. Using the Wilcoxon rank-sum test (Wilcoxon test), the study compared the IC50 values of 198 drugs between high-risk and the low-risk groups. This test was employed to identify the significant differences in drug sensitivity between the two groups.

Immune cell infiltration

CIBERSORT, a widely used computational tool in tumor immunology, was applied to quantitatively assess the relative proportions of 22 immune cell types in HNSCC samples, providing insights into the immune infiltration status of the tumors. The Wilcoxon test was employed to compare differences in immune infiltration scores among the 22 immune cell types, facilitating the identification of significant variations in immune cell infiltration between different groups.

Quantification of Immune Microenvironment Characteristics

To comprehensively analyze the tumor microenvironmental characteristics of HNSCC patients, the Wilcoxon test was employed to calculate the stromal scores, immune scores, microenvironmental scores, ESTIMATE scores, and tumor purity based on the TCGA-HNSCC dataset. The risk model, constructed using miRNAs and target genes identified in earlier analyses, was integrated with data derived from the R package ESTIMATE. This analysis utilized gene expression data from all tumor samples in the TCGA-HNSCC cohort to provide a deeper understanding of the association between tumor microenvironment characteristics and patient prognosis.

Quantification of Absolute Abundance of Immune Cells

To investigate the absolute abundance profiles of immune and stromal cells in HNSCC patient samples, the absolute abundance of 8 immune cell types and 2 stromal cell types was quantified. The R package MCPCounter, a tool designed for assessing the absolute abundance of different cell populations in the tumor microenvironment based on gene expression data, was employed to analyze these HNSCC samples. The Wilcoxon test was applied to analyze differences in cell population abundance, providing insights into the composition and presence of diverse immune and stromal cells within the tumor microenvironment.

Preparation and Characterization of RNA4WJ Nanoparticles

Computational modeling was used to predict the folding pattern of RNA4WJ nanoparticles as well as intra- and inter-RNA interactions. RNA building blocks were synthesized either chemically or via transcription using T7 polymerase. To facilitate labeling and tracking, an additional fluorescence imaging module, AF647, was incorporated into the RNA fragments. The RNA building blocks were subsequently assembled into RNA nanoparticles using a bottom-up approach, ensuring stability and structural integrity through precise assembly techniques and condition control. The fluorescence imaging module AF647 was also validated for stability and effectiveness. RNA fragments and RNA nanoparticles were purified to remove impurities. Finally, transmission electron microscopy (TEM) was performed to evaluate the size, morphology, and other key physicochemical properties of the RNA4WJ nanoparticles.

***In vitro* Experiments with RNA4WJ Nanoparticle**

Based on the screening of miRNAs and their target genes, a human tongue squamous carcinoma cell line (Cal27) was selected as the *in vitro* experimental model to investigate the stability, loading capacity, and targeting of RNA4WJ nanoparticles. In this study, a nuclease-resistant locked nucleic acid (LNA) 21 (LNA21, sequence: 5'-CAACATCAGTCTGATAAGCT-3'), designed to target human miR-21, was used to specifically inhibit the function of hsa-miR-21-5p. A negative control LNA (NC, sequence: 5'-GTGTAACACGTCTATACGCCCA-3') was employed as a control. LNA21, paclitaxel (PTX), and/or the EGFR ligand (EGFRapt) were incorporated into RNA4WJ nanoparticles to generate distinct nanoparticle formulations with varied loading profiles. Confocal microscopy, flow cytometry and cell proliferation assays were employed to evaluate the intracellular uptake efficiency and anti-tumor efficacy of RNA nanoparticles in cultured Cal27 cells. The cells were treated with

4WJ-AF647 or 4WJ-EGFRapt-AF647 nanoparticles at a concentration of 400 nM for 4 hours, followed by staining with iFluor 488 phalloidin to visualize F-actin and DAPI for nuclear staining. The fluorescent images were obtained by using an Olympus microscope. Additionally, the cells were exposed to the specified nanoparticles containing 500 nM LNA21 and/or 50 nM PTX for 24 hours. Cell viability and proliferation were subsequently evaluated using the CCK-8 assay, performed in accordance with the manufacturer's instructions.

In vivo Experiments with RNA4WJ Nanoparticles

To evaluate the *in vivo* targeting and anti-tumor efficacy of RNA4WJ nanoparticle, an animal model with a subcutaneous injection of 5×10^6 Cal27 cells into female 5-6 week-old nude mice was established. The targeting and biodistribution characteristics of near-infrared (NIR)-labeled RNA4WJ nanoparticles were assessed using an *in vivo* imaging system (IVIS, PerkinElmer) to monitor their biodistribution in tumor-bearing mice. Briefly, tumor-bearing mice were intravenously injected with 4WJ-AF647 or 4WJ-EGFRapt-AF647 nanoparticles, with PBS serving as the control. At 8-hour post-injection, the mice were euthanized via CO_2 overdose. Major organs were then harvested for fluorescence imaging (Ex = 640 nm, Em = 680 nm). Alternatively, one week after cell inoculation, the mice were randomly divided into 10 groups (n = 5 per group). The groups received the following treatments: PBS, PTX (10 mg/kg/week) via intravenous injection, or nanoparticles with different loading profiles (equivalent to 10 mg/kg PTX per week) via intravenous injection. The treatment period lasted for 4 weeks. Tumor volume was calculated using the formula (length × width^2/2) and monitored every four days. On Day 30 post treatment, the mice were sacrificed via CO_2 overdose.

RESULTS

Differential Expression Analysis of miRNA and RNA-Seq

This study conducted differential expression analyses of miRNAs using three datasets: TCGA-HNSCC, GSE28100, and GSE34496 (Fig. 2A). For the GSE28100 dataset from GEO, differential expression analysis between tumor and healthy samples was performed using the limma R package. A total of 56 miRNAs exhibited significant differential expression, with 11 downregulated and 45 upregulated. Similarly, analysis of the GSE34496 dataset revealed 35 significantly differentially expressed miRNAs, including 17 downregulated and 18 upregulated miRNAs. In the TCGA-HNSCC dataset, differential expression analysis was performed using DESeq2, identifying 363 significantly differentially expressed miRNAs, of which 163 were downregulated and 200 were upregulated.

After conducting intersection analysis of the differentially expressed miRNAs identified from the TCGA-HNSCC, GSE28100, and GSE34496 datasets, a total of 18 miRNAs were obtained. These differentially expressed miRNAs may be involved in key signaling pathways and regulatory networks associated with HNSCC development, progression, and treatment response. Additionally, differential expression analysis of genes in TCGA-HNSCC tumor and control samples was performed using DESeq2 software (Fig. 2B). This analysis identified 7,600 differentially expressed genes, including 3,188 down-regulated and 4,412 up-regulated genes. These results provide a comprehensive dataset for subsequent investigations into the molecular mechanisms underlying HNSCC.

DFS and OS Survival Analysis

DFS analysis was performed for each of the 18 differentially expressed miRNAs using the R package survminer. The analysis, based on the optimal cutpoint method, revealed that only the expression level of hsa-miR-21-5p showed a significant association with DFS outcomes. The optimal cutoff value for DFS analysis was determined using the surv_cutpoint function, with a cutpoint set at 264899.59. This value was used to divide the patients into high- and low-expression groups for further investigation. Patients in the high-expression group of hsa-miR-21-5p exhibited significantly poorer DFS compared to the low-expression group. The hazard ratio (HR) for the high-expression group was 0.47 (95% confidence interval (CI): 0.31-0.71), indicating higher risk of adverse survival events in this cohort. Statistical significance was confirmed using the log-rank test, with a p-value of 0.0004, further validating the prognostic relevance of hsa-miR-21-5p in HNSCC.

OA analysis was conducted to complement the DFS findings, as DFS and OS provide insights into different dimensions of patient survival. The analysis employed the optimal cutoff value method, with results showing that patients in the hsa-miR-21-5p high-expression group experienced poorer OS outcomes across 1-, 3- or 5-year survival intervals. This finding reinforces that high expression of hsa-miR-21-5p correlates with increased survival risk and a higher susceptibility to lethal events compared to the low-expression group (Fig. 2D). To further

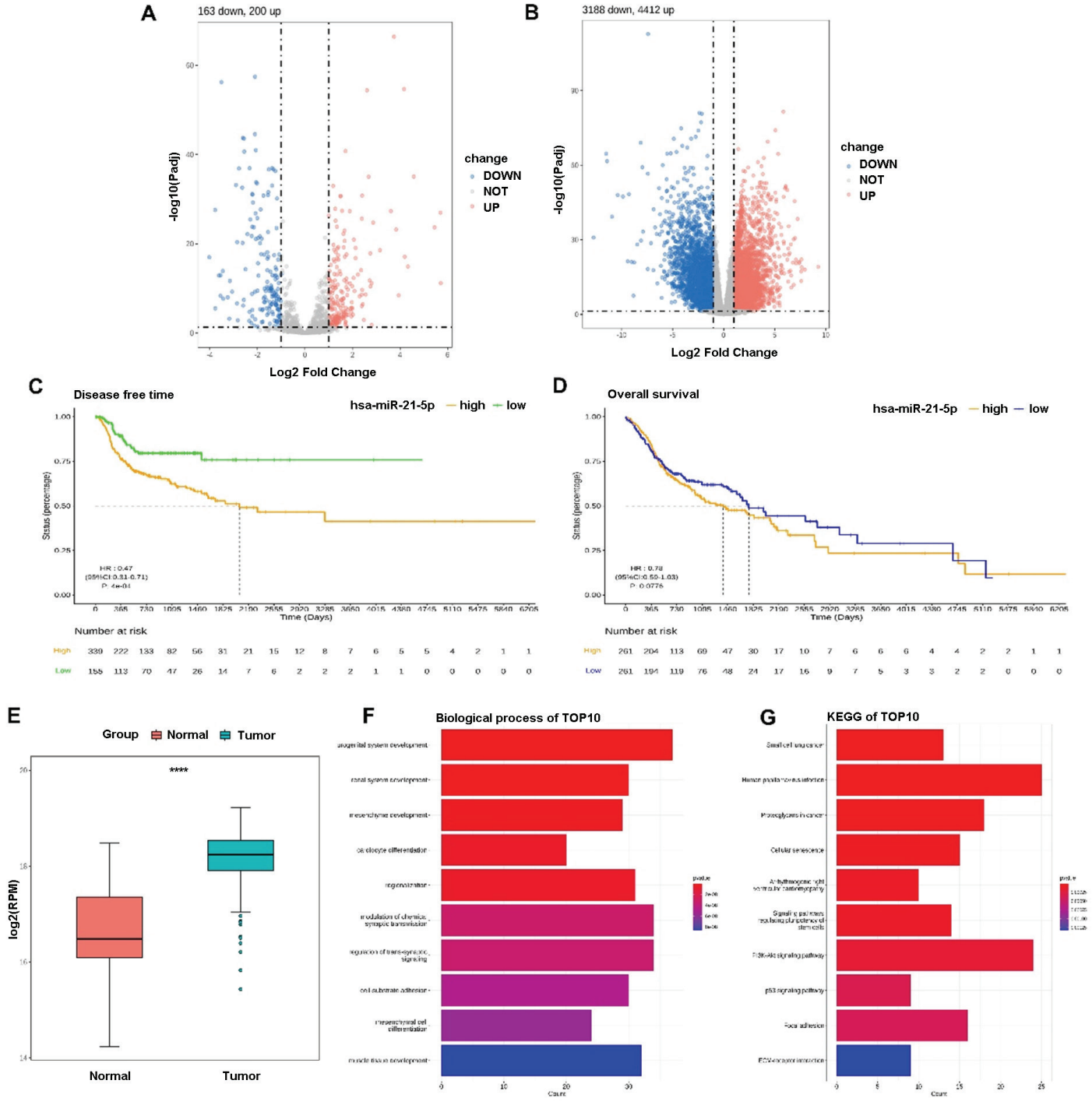

Fig. 2. High-throughput transcriptome gene sequencing analysis. (A) Volcano plot of differentially expressed miRNAs. (B) Volcano plot of differentially expressed genes. (C) Disease free survival (DFS) analysis using the optimal intercept method. (D) Overall survival (OS) analysis using the optimal intercept method. (E) Differential expression of hsa-miR-21-5p in tumor tissues and healthy tissues based on TCGA data. (F) GO biological process analysis of target genes. (G) KEGG pathway enrichment analysis of target genes. ****: $p<0.0001$.

validate these findings, a comparative analysis of hsa-miR-21-5p expression levels between HNSCC tissues and healthy tissues was performed using TCGA-HNSCC data. Statistical box plot analysis demonstrated significantly elevated hsa-miR-21-5p expression in HNSCC tissues compared to healthy controls (Fig. 2E). These results strongly indicate that the high expression of hsa-miR-21-5p is closely associated with tumorigenesis, progression, and its potential role as a prognostic biomarker in HNSCC.

Functional Analysis of Differentially Expressed miRNA Target Genes

TargetScan, miRDB, and miRTarBase were used to predict miRNA target genes, and 7,600 differentially expressed genes were analyzed as a reference set. This approach identified 836 differentially expressed miRNA target genes, including 381 up-regulated and 455 down-regulated genes. GO enrichment analysis and KEGG pathway analysis were conducted to annotate and characterize these genes in terms of biological processes, molecular functions, and cellular components.

GO Analysis

GO analysis identified the Top 10 enriched biological processes (Fig. 2F), providing insights into the development and progression of HNSCC. Notably, processes such as urogenital system development and renal system development suggest systemic metabolic and hormonal imbalances that may contribute to HNSCC risk. Additionally, lifestyle factors such as tobacco and alcohol consumption align with biological pathways linked to nutritional intake regulation, both key triggers of HNSCC. From a developmental perspective, abnormalities in mesenchymal cell differentiation (MCCD) highlight its role as a precursor for various tissues. Disruptions in spatial localization and differentiation of mesenchymal cells may lead to aberrant proliferation and differentiation of epithelial cells, promoting HNSCC formation.

KEGG Analysis

The top 10 pathways identified through KEGG analysis highlight critical mechanisms involved in the pathogenesis of HNSCC (Fig. 2G). These pathways include small cell lung cancer, human papillomavirus infection, proteoglycans in cancer, cellular senescence, arrhythmogenic right ventricular cardiomyopathy, stem cell pluripotency regulation signaling pathway, PI3K-Akt signaling pathway, p53 signaling pathway, focal adhesion, and extracellular matrix-receptor interactions. These findings underscore the complexity and multifaceted nature of HNSCC development, offering insights into the molecular pathways that could serve as potential therapeutic targets or diagnostic markers.

LASSO-COX Modeling of hsa-miR-21-5p Target Genes

To elucidate the role of hsa-miR-21-5p in HNSCC, its target genes were analyzed using the LASSO-COX model (Fig. 3A-D). The LASSO (Least Absolute Shrinkage and Selection Operator) algorithm was employed for feature selection, narrowing down 21 candidate genes to those with the highest predictive value for survival analysis. Cross-validation determined the optimal regularization parameter (λ), after which the model was refitted to derive the coefficients for each gene. As a result, six genes, including JPH1, EPM2A, DDAH1, NFIA, SATB1, and NTF3, were identified as significantly influencing patient survival. These findings enhance the predictive accuracy and interpretability of the survival model.

Survival analysis of target genes

hsa-miR-21-5p emerged as a potential prognostic marker for HNSCC, prompting a detailed exploration of its target genes. Analysis revealed that 21 genes were upregulated in samples with downregulated hsa-miR-21-5p, underscoring its regulatory role. A Cox model incorporating hsa-miR-21-5p and its target genes identified 6 key genes-JPH1, EPM2A, DDAH1, NFIA, SATB1, and NTF3-for DFS and OS analyses (Fig. 3E).

For JPH1 and EPM2A, optimal cutoff values (4.88 and 0.37, respectively) were established to stratify patients into high- and low-expression groups. DFS survival analysis for JPH1 and EPM2A expression levels revealed poorer outcomes in the high-expression group, with hazard ratios (HRs) of 0.69 and 0.71, respectively (Fig. S1-S2). Survival data at 1, 3, and 5 years further confirmed that patients in the high-expression group had a higher risk of adverse survival events compared to the low-expression group. OS analysis further demonstrated similar results. While studies on DDAH1's role in tumorigenesis and progression are limited, in this study, its aberrant expression in certain cancers has been associated with malignancy and prognosis (Fig. S3). NFIA aberrations may be linked to tumor proliferation, metastasis, and invasion capacity (Fig. S4). SATB1, overexpressed in various cancers such as breast cancer and HNSCC, is strongly associated with tumor progression, metastasis, and prognosis (Fig. S5). NTF3, involved in neurite growth and synapse formation, may impact tumor angiogenesis and resistance to treatment when aberrantly expressed (Fig. S6).

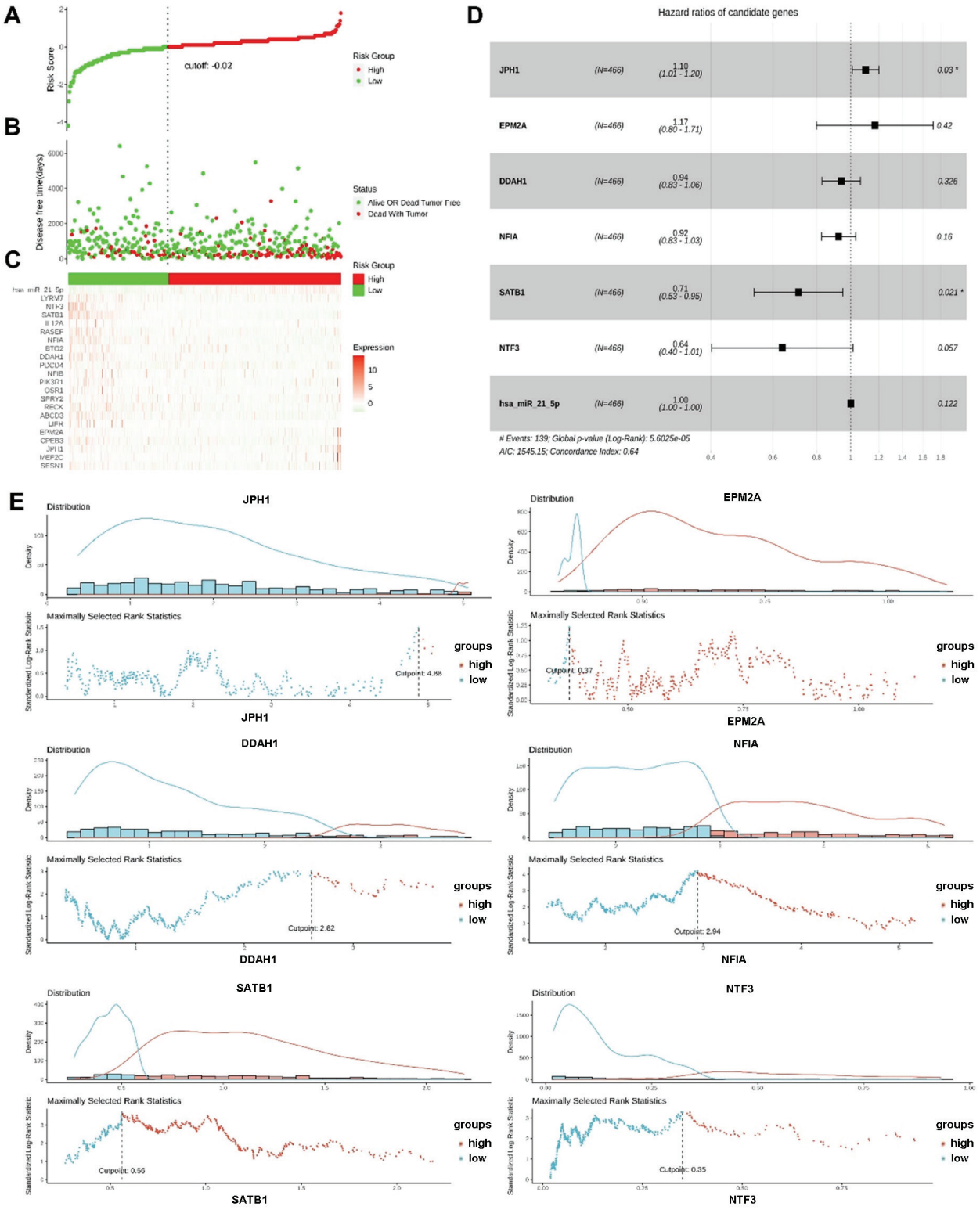

Fig. 3. LASSO-COX modeling of hsa-miR-21-5p target genes and survival analysis. (A) Cutoff division of target genes. (B) Disease free survival (DFS) analysis. (C) Expression levels of key genes. (D) Hazard ratio (HR) analysis of miRNA and their target genes. (E) Cutpoint analysis of key target genes, including JPH1, EPM2A, DDAH1, NFIA, SATB1, and NTF3.

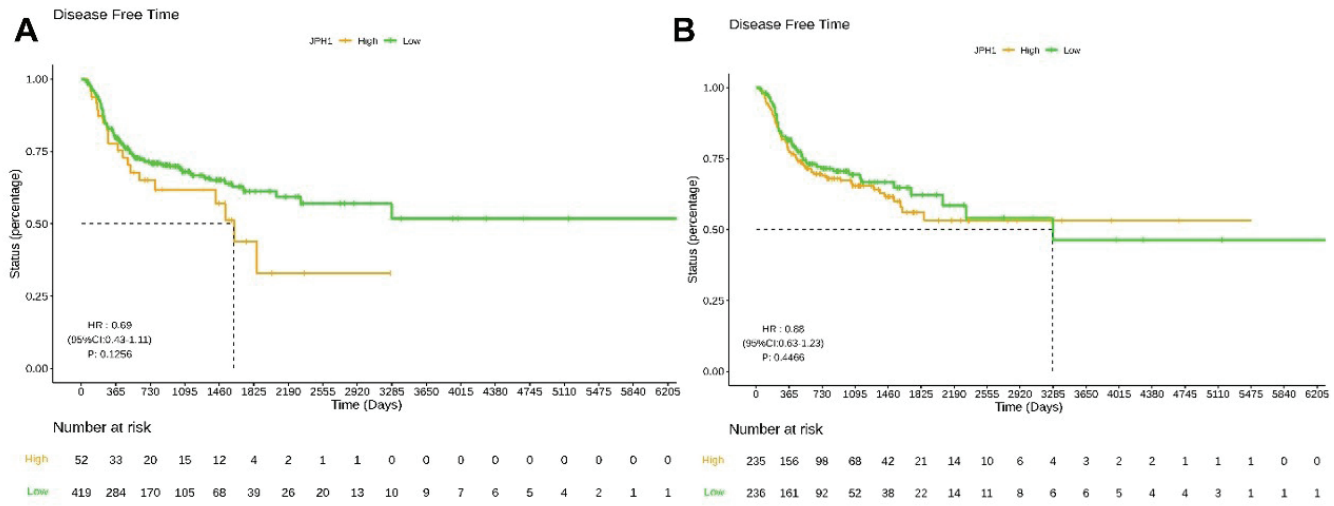

Fig. S1. Disease free survival (DFS) and overall survival (OS) analyses of patients with different JPH1 expression levels.

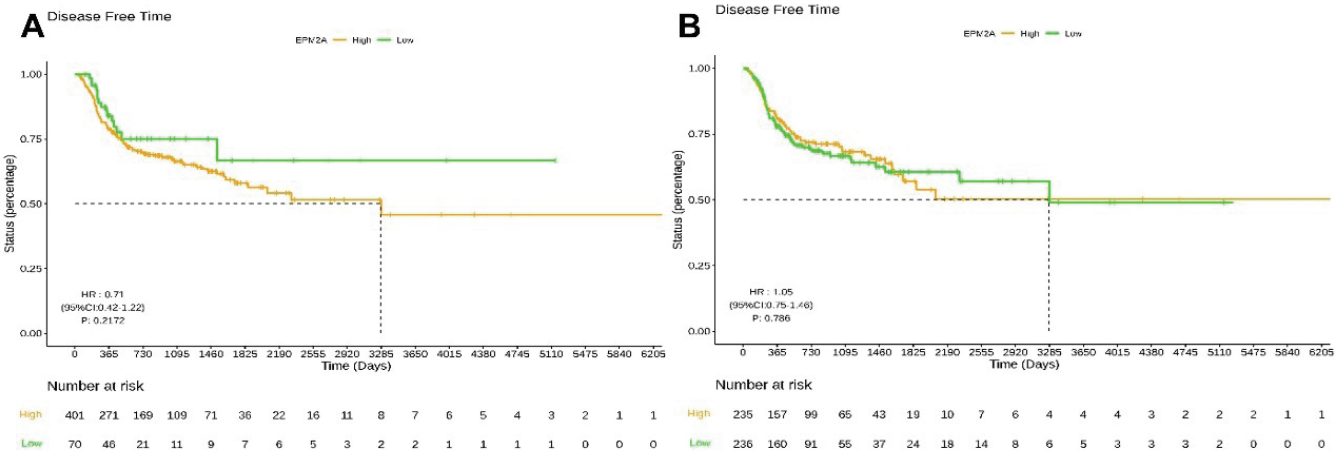

Fig. S2. Disease free survival (DFS) and overall survival (OS) analyses of patients with different EPM2A expression levels.

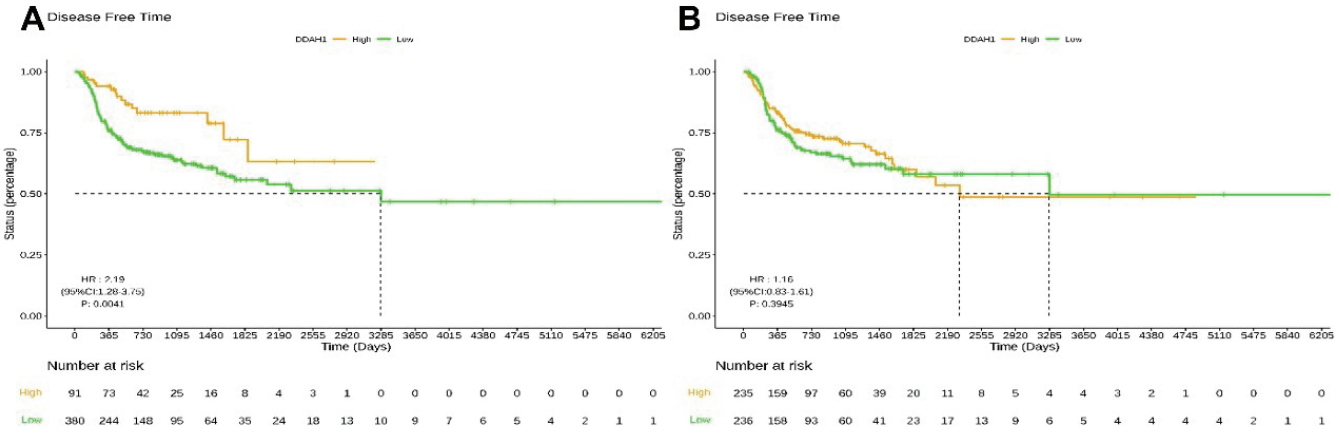

Fig. S3. Disease free survival (DFS) and overall survival (OS) analyses of patients with different DDAH1 expression levels.

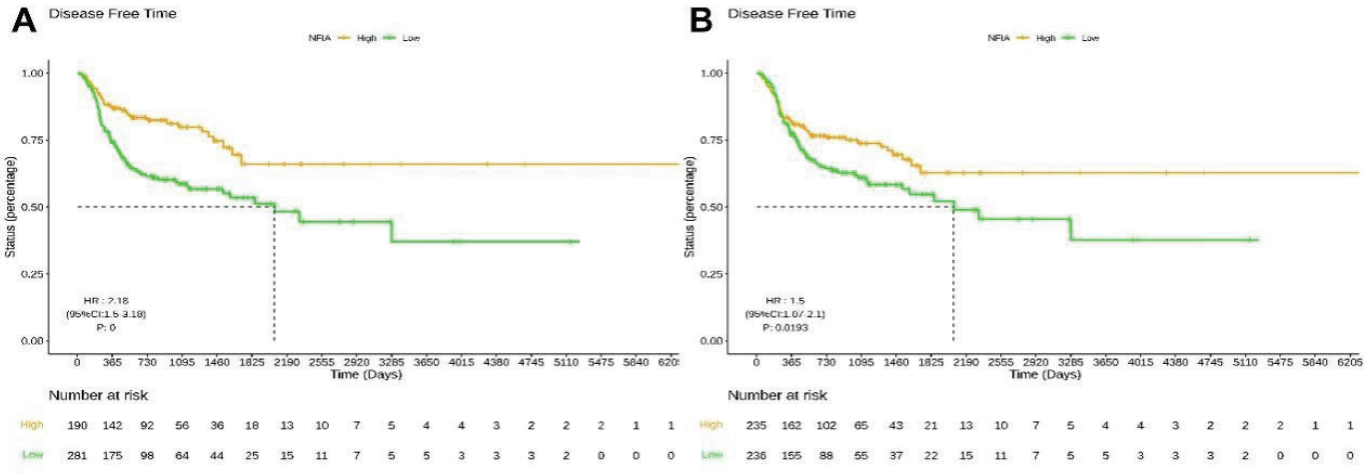

Fig. S4. Disease free survival (DFS) and overall survival (OS) analyses of patients with different NFIA expression levels.

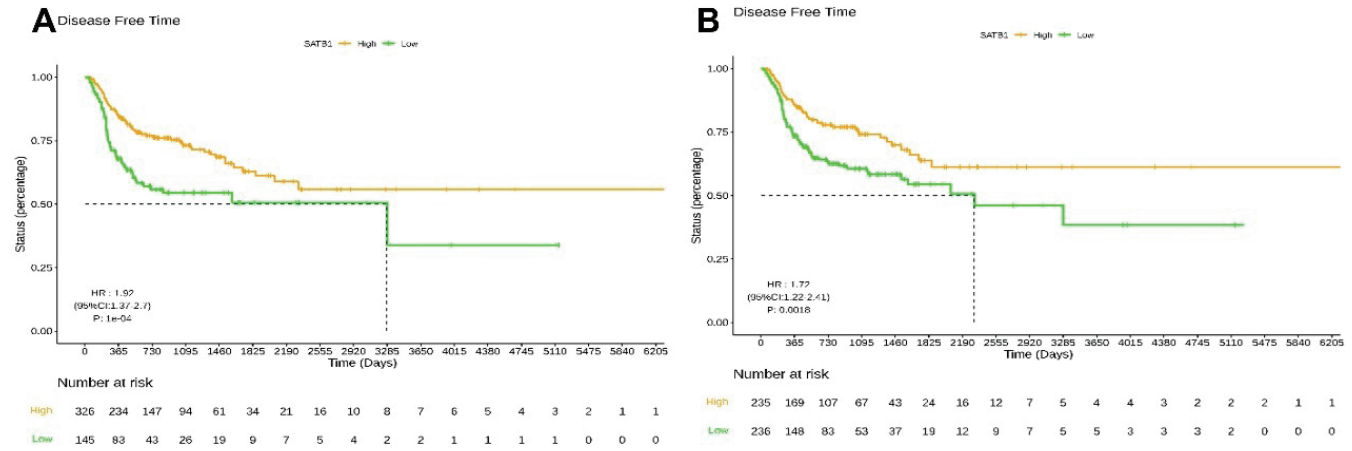

Fig. S5. Disease free survival (DFS) and overall survival (OS) analyses of patients with different SATB1 expression levels.

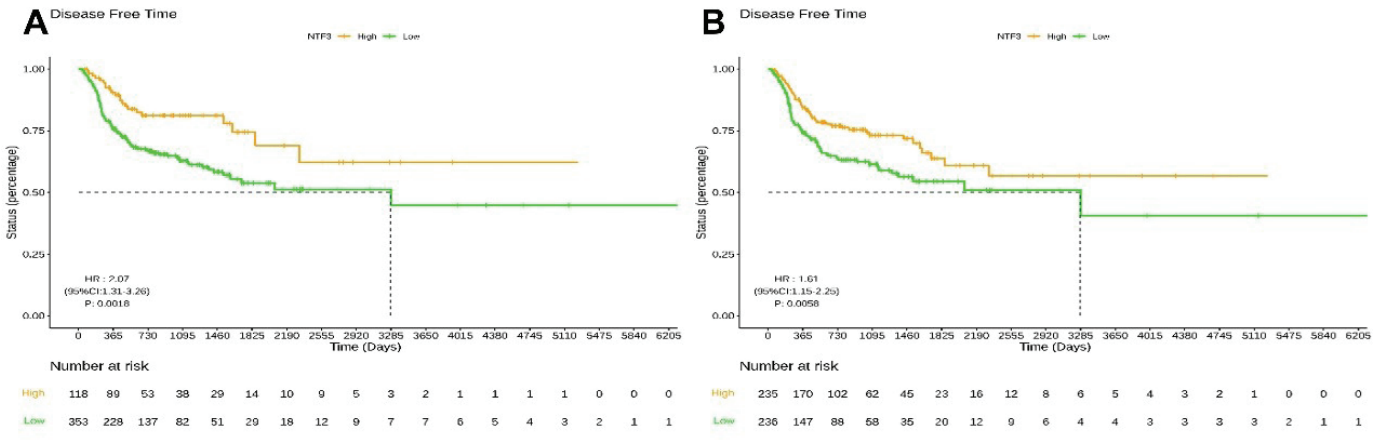

Fig. S6. Disease free survival (DFS) and overall survival (OS) analyses of patients with different NTF3 expression levels.

Drug Sensitivity Analysis

An in-depth drug sensitivity analysis was performed using the oncoPredict software package and the GDSC database (Fig. 4). A total of 198 drugs were analyzed, and their sensitivities were compared between high- and low-risk groups, categorized based on hsa-miR-21-5p and the 6 target gene risk models. The IC50 values of the drugs were evaluated using the Wilcoxon test. The results identified 38 drugs as potential candidates for low-risk groups, indicating that these drugs might offer better therapeutic efficacy for low-risk patients. Additionally, 60 drugs were identified as suitable for high-risk groups, suggesting their enhanced effectiveness in patients at higher risk.

Violin plots were used to visualize the IC50 distributions of these drugs across the two groups, providing a clear and intuitive comparison. This analysis offers valuable insights for clinicians, helping in the selection of more effective treatment strategies tailored to the risk profiles of individual patients.

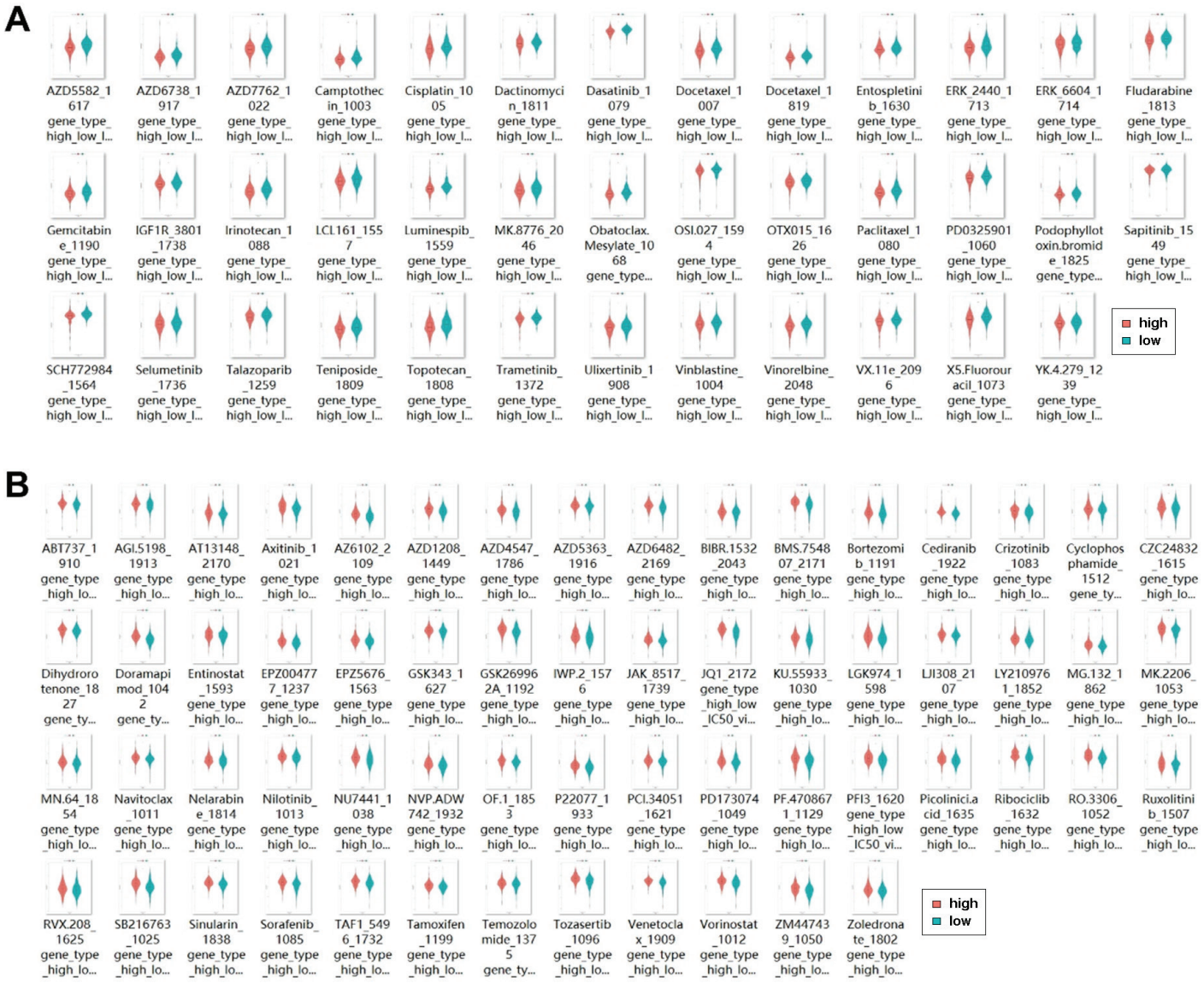

Fig. 4. Drug sensitivity analysis of IC50 values using the Wilcoxon test. The sensitivities were compared between high- and low-risk groups based on hsa-miR-21-5p and the 6 target gene risk models. (A) Drugs as potential candidates for low-risk groups. (B) Drugs as potential candidates for high-risk groups.

Immune Cell Infiltration

The composition of 22 immune cell types was analyzed using the CIBERSORT software package (Fig. 5A). By integrating the risk model of hsa-miR-21-5p and its target gene composition with immune infiltration characteristics, samples were divided based on the risk score corresponding to the maximum AUC value from the ROC curve. Subsequently, Differential analysis of immune cell infiltration scores was conducted using the Wilcoxon test. Significant differences in the infiltration scores of several immune cell types, including macrophages M1, T follicular helper cells, naïve B cells, resting NK cells, plasma cells, regulatory T cells (Tregs), neutrophils, activated NK cells, and gamma delta T cells, were observed between high- and low-risk patients with HNSCC.

Stromal and Immune Score Calculation

The Wilcoxon test results demonstrated significant differences in stromal score, immune score, ESTIMATEScore, and tumor purity between high- and low-risk HNSCC patients (Fig. 5B, C). These findings reveal the variability in the tumor microenvironment across risk groups, providing important insights for investigating tumor development mechanisms and advancing personalized treatment approaches. The stromal score assesses the extent of connective tissue and blood vessel formation surrounding the tumor, while the immune score represents the level of immune cell infiltration within tumor tissues. Significant differences in these scores between high- and low-risk groups suggest a profound influence on tumor growth, progression, and response to therapy.

Calculation of Absolute Abundance of Immune Cells

The absolute abundance of 8 immune cells, including T cells, CD8+ T cells, cytotoxic lymphocytes, NK cells, B cell lineage, monocytes, myeloid dendritic cells, and neutrophils, and 2 stromal cells, inducing endothelial cells and fibroblasts, was evaluated using the MCPCounter R package, based on gene expression levels from TCGA-HNSCC samples (Fig. 5D). The results showed the low-risk group exhibited a significantly higher abundance of these immune and stromal cells compared to the high-risk groups. This difference indicates that the low-risk group may benefit from a more robust immune response and enhanced immune surveillance. In contrast, the reduced immune cell abundance in the high-risk group could contribute to an immunosuppressive state and facilitate immune escape mechanisms.

Differential Expression of has-miR-21-5p

The differential expression of the miRNA hsa-miR-21-5p and its target gene (NTF3) was validated using *in situ* hybridization (ISH) and immunohistochemistry (IHC) analyses on tissue sections (catalog number: HOraC060PG01, Shanghai Outdo Biotechnology Co., Ltd). This study included 56 patients with oral cancer, including 55 cancerous tissue samples and 5 paracancerous epithelial samples, with each specimen taken from a distinct point. Tissue sections had a diameter of 2.0 mm and a thickness of 4 μm. The results revealed significantly elevated expression of hsa-miR-21-5p (Fig. 6A), along with its target gene NTF3 (Fig. 6B, C), in cancerous tissues compared to paracancerous tissues. These findings suggest a pivotal role for hsa-miR-21-5p in the development and progression of oral cancer, potentially through its regulation of target gene. Moreover, the observed heterogeneity in expression patterns reflects the molecular diversity of oral cancer, highlighting the importance of personalized approaches to diagnosis and treatment.

***In vitro* Delivery and anti-tumor effects of RNA4WJ Nanoparticles**

Following the screening of hsa-miR-21-5p targets, 4WJ-AF647 and 4WJ-EGFRapt-AF647 nanoparticles containing EGFR ligand were characterized with diameters ranging from 10 to 20 nm (Fig. 7A, B). Human tongue squamous carcinoma cell line (Cal27) primarily employs integrin were selected for *in vitro* experiments to evaluate the targeting efficiency and intracellular uptake of these RNA nanoparticles. Confocal microscopy and flow cytometry analyses confirmed effective cellular uptake and targeting by 4WJ-EGFRapt-AF647 nanoparticles (Fig. 7C, Fig. S7). Cell viability assays revealed no significant difference in survival rates between the control and 4WJ-NC groups, indicating minimal cytotoxic effects of the 4WJ-NC nanoparticles (Fig. 7D). However, a significant decrease in cell viability was observed in the 4WJ-LNA21 group compared to the 4WJ-NC group, demonstrating a significant inhibitory effect on HNSCC cell survival. These findings suggest that the addition of LNA21 enhances the therapeutic efficacy of RNA nanoparticles. Collectively, the results highlight the potential of RNA4WJ nanoparticles as a therapeutic strategy for targeting HNSCC cells, underscoring their capability for effective cellular interaction and antitumor activity.

To enhance therapeutic efficacy, PTX was incorporated into RNA4WJ nanoparticles, and *in vitro* delivery experiments were conducted (Fig. 7E). Significant

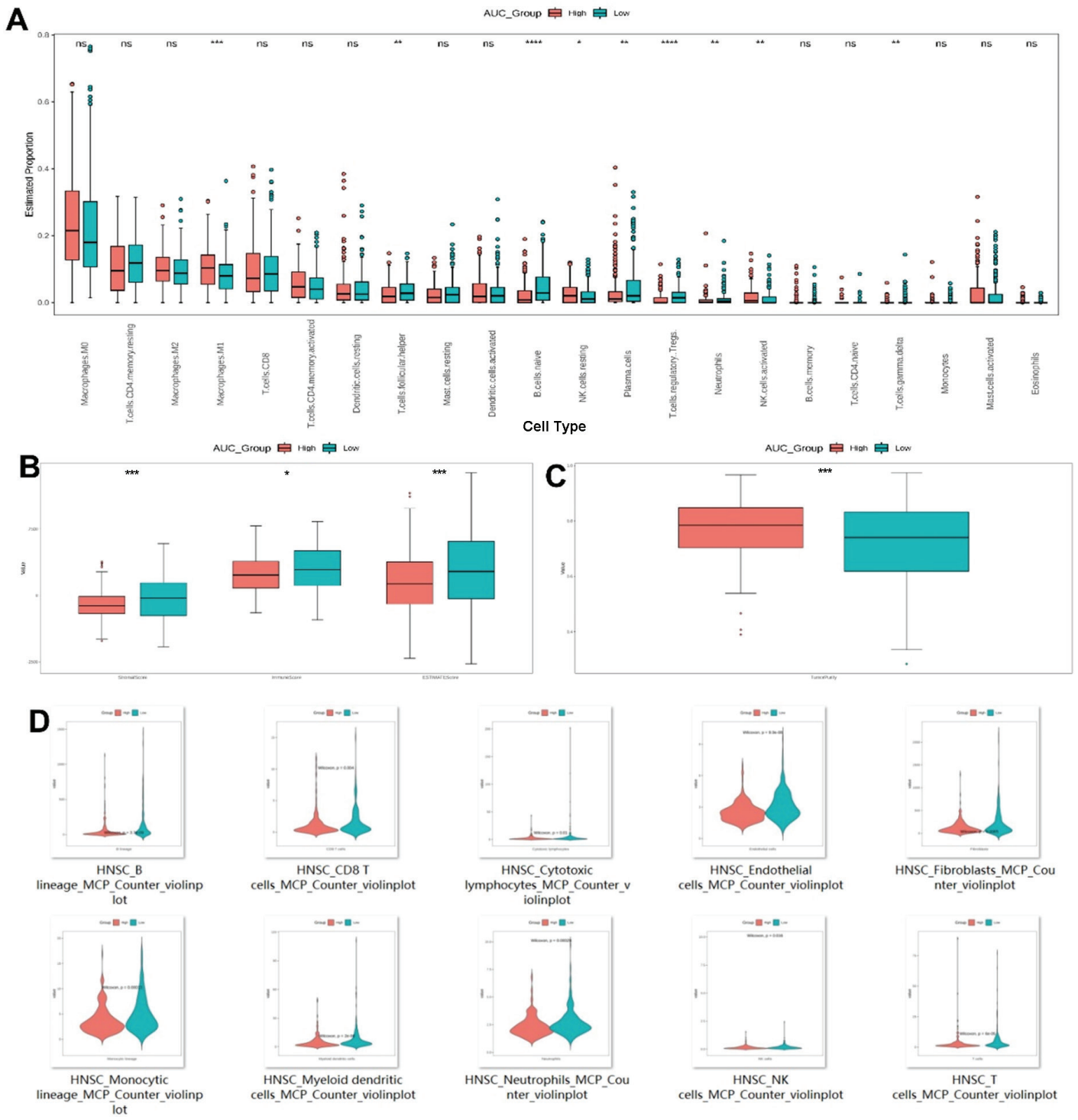

Fig. 5. Analysis of immune responsiveness. (A) Differences in the infiltration of 22 immune cell types between high-risk and low-risk groups. (B) Stromal scores for high-risk and low-risk groups. (C) Immune scores for high-risk and low-risk groups. (D) Combined stromal and immune scores for high-risk and low-risk groups. *: $p<0.05$, ***: $p<0.001$.

differences were observed between the 4WJ and 4WJ-PTX groups, as well as between the 4WJ-NC-PTX and 4WJ-LNA21-PTX groups. The observed difference between the 4WJ and 4WJ-PTX groups indicates that the incorporation of PTX modifies the nanoparticles' mechanism of action, thereby enhancing their therapeutic potential. Additionally, the difference between the 4WJ-NC-PTX and 4WJ-LNA21-PTX groups highlights the potential impact of hsa-miR-21-5p variants on the targeting efficiency and intracellular effects of the nanoparticles. These results underscore the importance of PTX loading and miRNA selection in optimizing the therapeutic efficacy of RNA4WJ nanoparticles for cancer treatment.

In vivo Delivery anti-tumor effects of RNA4WJ Nanoparticles using tumor-bearing nude mice

In vivo experiments were conducted to evaluate the delivery efficiency of RNA4WJ nanoparticles in nude mice bearing Cal27 tumors. Comparisons were made between 4WJ-AF647 nanoparticles and 4WJ-EGFRapt-AF647 nanoparticles containing EGFR ligand. The addition of the EGFR ligand enhanced the selectivity of the nanoparticles for EGFR, thereby improving their targeting and intracellular uptake efficiency, which were prominently observed fluorescence in Cal27 tumors (Fig. 8A).

To further investigate therapeutic efficacy, PTX was incorporated into the RNA4WJ nanoparticles. Comparisons between 4WJ-PTX nanoparticles and 4WJ-EGFRapt-PTX nanoparticles revealed that the combination of PTX with EGFR ligand-functionalized nanoparticles further improved drug targeting and anti-tumor efficacy (Fig. 8B). Similarly, the therapeutic efficacy of 4WJ-LNA21 nanoparticle was compared with

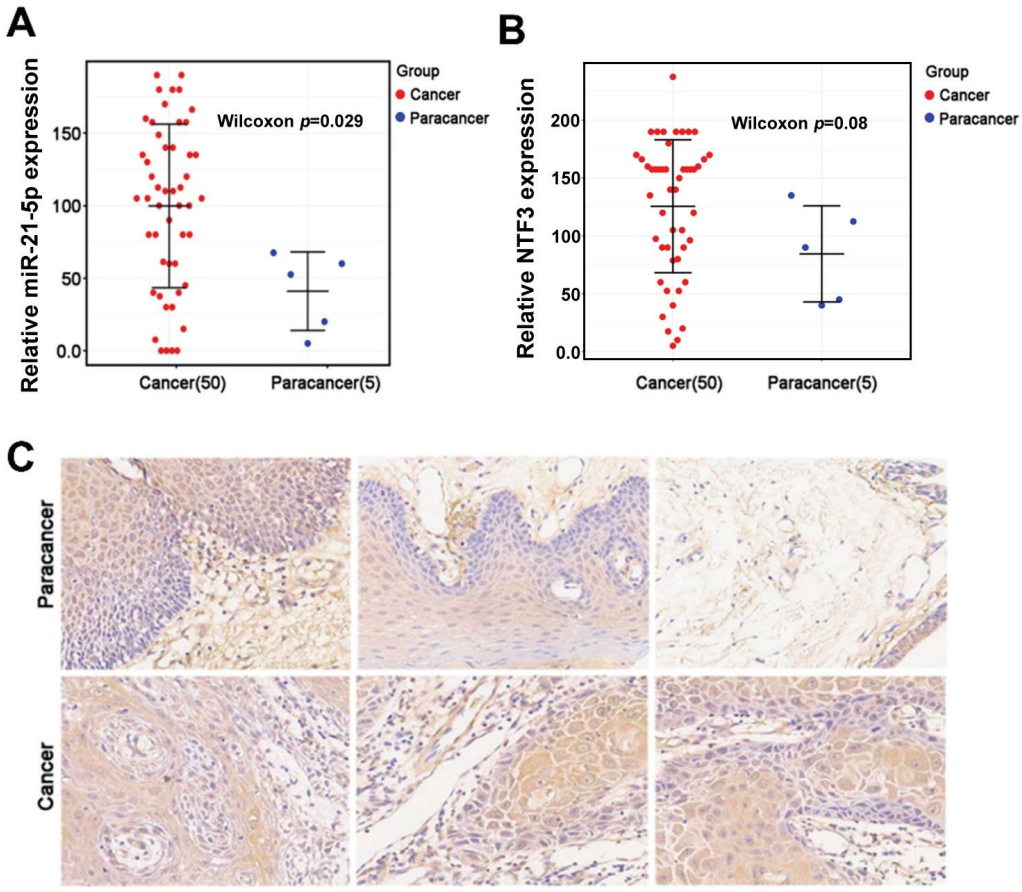

Fig. 6. Validation of the expression of hsa-miR-21-5p and its target gene NTF3 in oral cancer tissue sections using *in situ* hybridization (ISH) and immunohistochemistry (IHC) analyses. (A) The expression of hsa-miR-21-5p in cancerous tissues and paracancerous tissues. (B) The expression of target gene NTF3 in cancerous tissues and paracancerous tissues. (C) Representative IHC images of NTF3 in paracancerous and cancerous tissues.

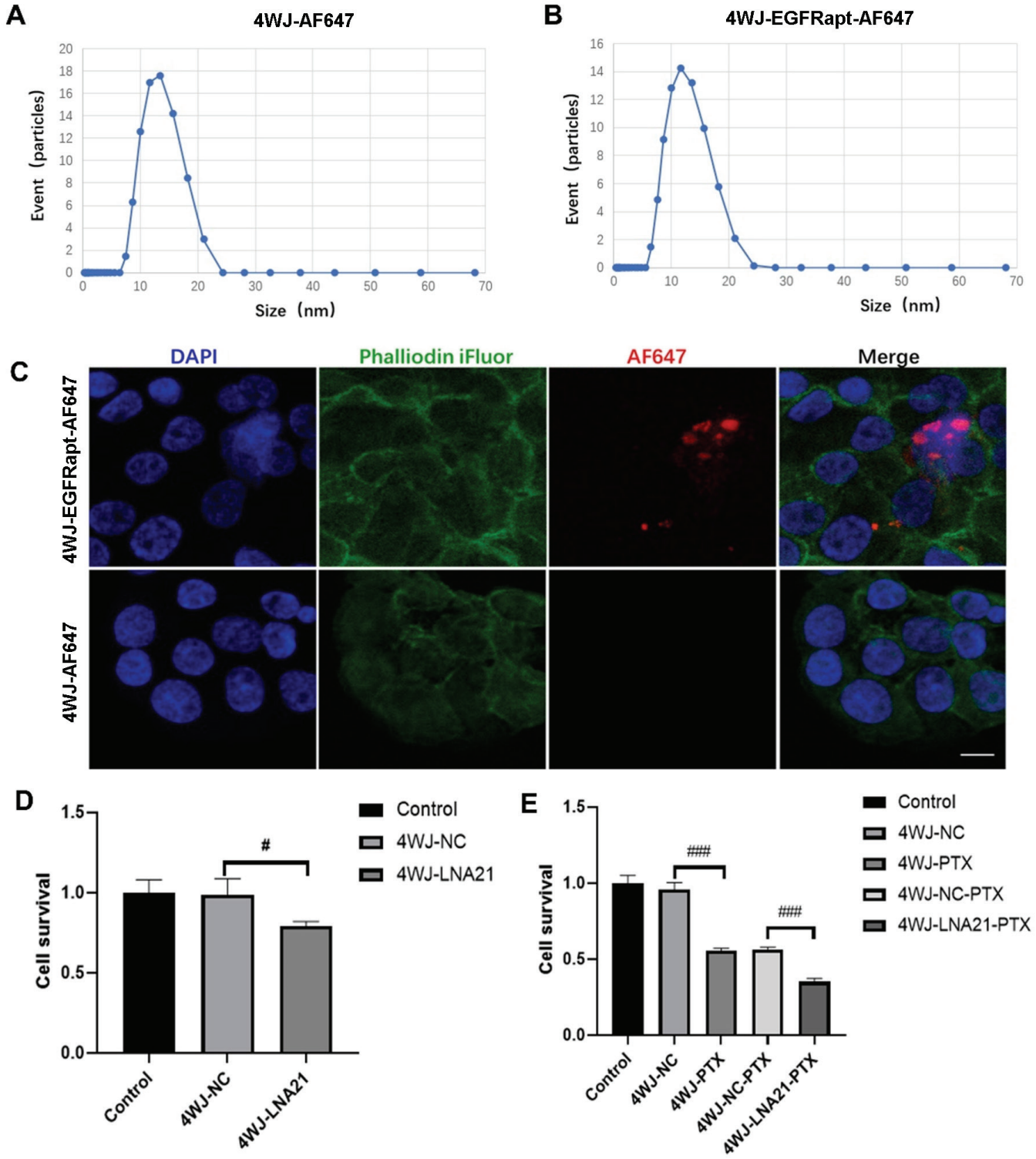

Fig. 7. *In vitro* delivery experiments using RNA4WJ nanoparticles with or without PTX. (A) Size distribution of 4WJ-AF647 nanoparticles. (B) Size distribution of 4WJ-EGFRapt-AF647 nanoparticles. (C) Confocal microscopy showing EGFR ligand-labeled nanoparticles specifically binding to Cal27 cells. Scale bar: 20 μm. (D) *In vitro* delivery efficiency of RNA4WJ nanoparticles incorporating with LNA21 or NC. (E) *In vitro* delivery efficiency of RNA4WJ nanoparticles with added PTX and/or LNA21. Student's t-Test. #: $p<0.05$, ###: $p<0.001$.

4WJ-EGFRapt-LNA21 nanoparticles. The inclusion of the EGFR ligand in the latter formulation enhanced miRNA-targeted modulation and anti-tumor efficacy. Among the experimental groups, the RNA4WJ formulation without additional functionalization demonstrated the least efficacy in suppressing tumor size (Fig. 8B). In contrast, the 4WJ-EGFRapt-LNA21-PTX group exhibited the most pronounced therapeutic effect, achieving the greatest reduction in tumor size (Fig. 8B). These findings highlight the potential of multifunctional nanoparticle systems in enhancing the efficacy of combination therapy and provide valuable insights for the treatment and management of HNSCC.

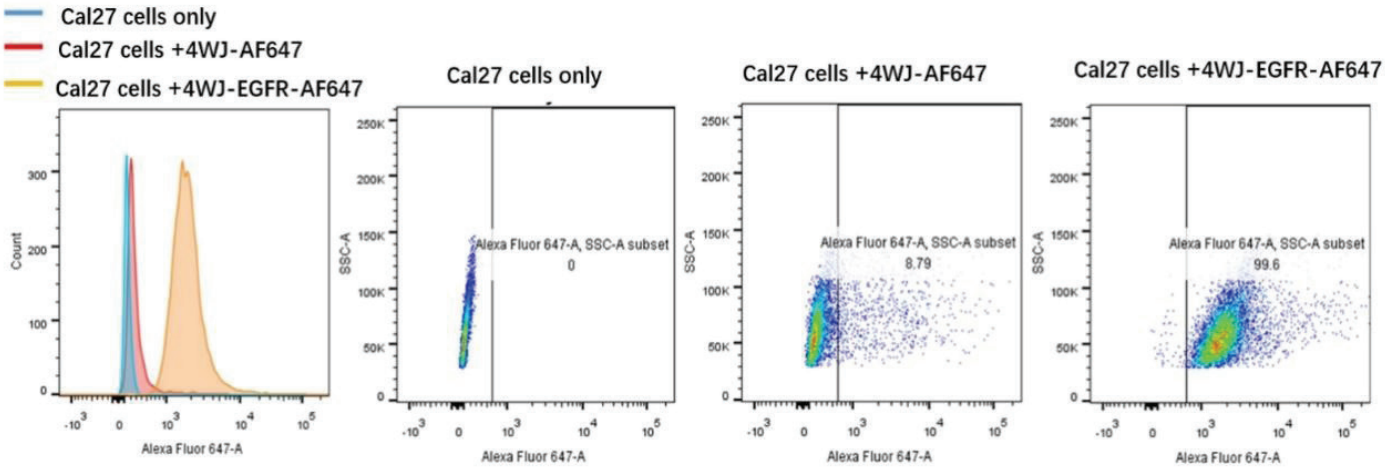

Fig. S7. Evaluation of the intracellular uptake efficiency of Cal27 cells by flow cytometry analysis. Cal27 cells with PBS, 4WJ-AF647, or 4WJ-EGFRapt-AF647 treatments were subjected to flow cytometry.

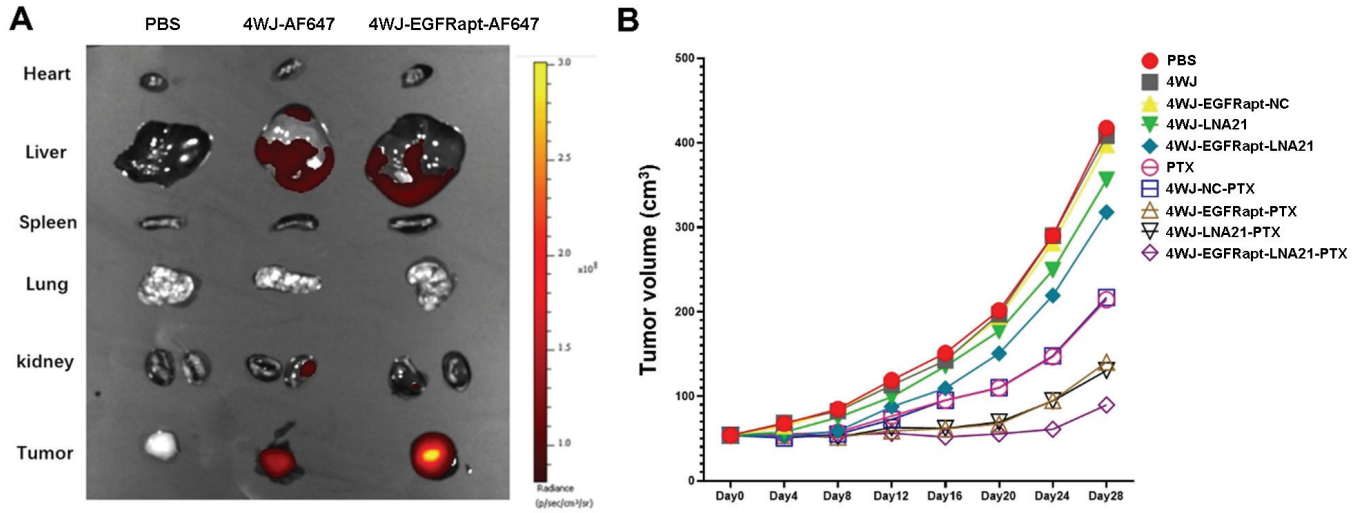

Fig. 8. *In vivo* delivery experiments using RNA4WJ nanoparticles with differing loading profiles in a mouse model. (A) *In vivo* distribution of targeted nanoparticles in tumor-bearing nude mice. The mice were intravenously injected with indicated nanoparticles for 8 hours. Major organs were harvested for fluorescence imaging using IVIS imaging system (Ex = 640 nm, Em = 680 nm). (B) Tumor volume variations at different time points post-treatment (n = 5 per group). The mice were received PBS, PTX (10 mg/kg/week) via intravenous injection, or nanoparticles with different loading profiles (equivalent to 10 mg/kg PTX per week) via intravenous injection. The treatment period lasted for 4 weeks.

DISCUSSION

The advent of miRNA-Seq and RNA-Seq technologies has revolutionized genomics research by providing a high-resolution platform for examining the expression profiles of miRNAs and mRNAs. These advancements have substantially improved our understanding of gene regulatory networks and their roles in disease progression[19]. In this study, datasets from the TCGA and GEO databases were utilized for an in-depth analysis. The miRNA-Seq dataset comprised 569 samples, including 525 HNSCC tumor samples and 44 normal control samples. Similarly, the RNA-Seq dataset included 546 samples, with 502 tumor samples and 44 normal controls. By integrating and analyzing these datasets, this study systematically examined the expression patterns of miRNAs and mRNAs in HNSCC.

A set of 18 miRNAs with significant regulatory roles in HNSCC was identified through a comprehensive analysis of differential miRNA expression across three datasets: TCGA-HNSCC, GSE28100, and GSE34496. These miRNAs are implicated in key signaling pathways and regulatory networks involved in HNSCC development, progression, and treatment. Notably, hsa-miR-21-5p emerged as a significant prognostic indicator, suggesting its pivotal involvement in the progression and outcomes of HNSCC. Additionally, DFS and OS analyses were conducted to comprehensively evaluate the prognostic impact of hsa-miR-21-5p. Comparative expression analysis using TCGA-HNSCC data revealed elevated expression of hsa-miR-21-5p in tumor tissues, correlating with tumor initiation and progression, which are consistent with previous reports[20].

HNSCC, a malignant tumor arising from the mucosal epithelial tissues of the head and neck, is driven by complex biological processes and diverse molecular mechanisms[21]. In this study, GO and KEGG pathway analyses identified critical biological processes, molecular functions, and pathways, including the PI3K-Akt and p53 signaling pathways, contributing to a deeper understanding of HNSCC pathogenesis and therapeutic opportunities. The LASSO-Cox model further refined these analyses by selecting six significant genes (JPH1, EPM2A, DDAH1, NFIA, SATB1, and NTF3) from a pool of 21 target genes associated with hsa-miR-21-5p. Among these, a specific interaction between hsa-miR-21-5p and NTF3 was observed (data not shown). miR-21 ISH and NTF3 IHC staining in cancerous and paracancerous tissue samples confirmed their direct relationship in oral cancer. This study also integrated miRNA and gene expression data from TCGA-HNSCC to construct a robust risk score formula, enabling precise prognostic predictions and guiding personalized treatment[22]. Consequently, hsa-miR-21-5p emerges as a key prognostic marker, with its target genes offering actionable insights into therapeutic approaches[23].

Drug sensitivity analysis revealed significant IC50 differences between high- and low-risk patient groups for 198 drugs, offering a practical reference for clinicians. Immune infiltration analysis identified variations in immune cell compositions, such as macrophages (M1), follicular helper T cells, and naive B cells, providing insights into the immune escape mechanisms in HNSCC[24]. Additionally, stromal and immune scores highlighted tumor microenvironment differences, crucial for understanding HNSCC biology and therapeutic responses[25].

The study also explored the application of RNA4WJ nanoparticles, a novel nanocarrier characterized by exceptional stability, biocompatibility, and targeting capabilities[26]. PTX, a widely used anticancer agent, demonstrates favorable therapeutic effects both as a free drug and when loaded into nanoparticles[27, 28]. In this study, RNA4WJ nanoparticles were co-loaded with a miR-21-5p inhibitor and PTX, achieving significant anti-tumor efficacy in both *in vitro* and *in vivo* models. In addition, EGFR-targeted therapies have demonstrated significant clinical efficacy in treating HNSCC[29, 30]. Here, the EGFR ligand, LNA21, and PTX loaded in RNA4WJ nanoparticles resulted in the most potent tumor suppression, highlighting the synergistic effects of targeted miRNA delivery and chemotherapeutic drug therapy. However, further investigation is required to validate the expression of NTF3 in tumor tissues following treatment with these nanoparticle formulations, as this would strengthen the current bioinformatics analysis. Collectively, by leveraging RNA4WJ nanoparticles and miRNAs, this study developed an innovative nanoparticle-based miRNA therapeutic strategy for precision treatment of HNSCC, offering a promising avenue to improve patient outcomes.

CONCLUSION

In this study, an efficient LASSO-COX screening model was developed using data mining and bioinformatics approaches to identify miRNA-mRNA interaction pairs with potential therapeutic value. The model considered various factors, including miRNA expression levels, regulatory networks, and interactions

with target mRNAs, providing more precise targeting options for personalized treatment of HNSCC. To validate the findings, human tongue squamous carcinoma cell line was used both *in vitro* and *in vivo* to evaluate the targeting and anticancer effects of RNA4WJ nanoparticles carrying PTX, EGFR ligand and therapeutic inhibitor for miR-21-5p. The results of this study are expected to contribute to the development of innovative and effective treatment approaches for HNSCC in clinical settings.

FUNDING

This work was supported by the National Natural Science Foundation of China (Grant No. 82301025), the Talents Introduction of Guangdong Provincial People's Hospital (Grant Nos. KY0120220255, 3227100558 and 8237030185), Guangzhou Municipal Science and Technology Bureau (Grant No. 2024A04J4888), the National Key Research and Development Program of China (Grant No. 2023YFC2413600).

CONFLICT OF INTEREST

The authors declare that no conflicting interests exist .

REFERENCES

1. Rosen R *et al* and Nickel C, Katsoulakis E, Mifsud M. Risk, prevention, screening and management of carotid artery stenosis in head & neck cancer patients-An evidence based review. *Oral Oncol.* 2024 Sep; 156: 106876. doi: 10.1016/j.oraloncology.2024.106876. PMid:38908097
2. Armache M *et al* and Leader AE, Fakhry C, Mady LJ. Readability of Patient Education Materials in Head and Neck Cancer: A Systematic Review. *JAMA Otolaryngol Head Neck Surg.* 2024 Aug 1; 150 (8): 713-724. doi: 10.1001/jamaoto.2024.1569. PMid:38900443
3. Li H *et al* and Mehra S, Osborn HA, Judson B. Association of Human Papillomavirus Status at Head and Neck Carcinoma Subsites with Overall Survival. *JAMA Otolaryngol Head Neck Surg.* 2018 Jun 1; 144 (6): 519-525. doi: 10.1001/jamaoto.2018.0395. PMid:29801040 PMCid:PMC6583856
4. Cancer Genome Atlas Network. Comprehensive genomic characterization of head and neck squamous cell carcinomas. *Nature*. 2015 Jan 29; 517 (7536): 576-82. doi: 10.1038/nature14129. PMid:25631445 PMCid:PMC4311405
5. Mattick JS *et al* and Wan Y, Wilusz JE, Wu M. Long noncoding RNAs: definitions, functions, challenges and recommendations. Nat Rev Mol Cell Biol. 2023 Jun; 24 (6): 430-447. doi: 10.1038/s41580-022-00566-8. PMid:36596869 PMCid:PMC10213152
6. Carron J *et al* and Ortega MM, Lima CSP, Lourenço GJ. microRNAs deregulation in head and neck squamous cell carcinoma. *Head Neck*. 2021 Feb; 43 (2): 645-667. doi: 10.1002/hed.26533. PMid:33159410
7. Dioguardi M *et al* and Ballini A, Lo Muzio L, Troiano G. The Potential microRNA Prognostic Signature in HNSCCs: A Systematic Review. *Noncoding RNA*. 2023 Sep 14; 9 (5): 54. doi: 10.3390/ncrna9050054. PMid:37736900 PMCid:PMC10514860
8. Piotrowski I *et al* and Golusiński W, Masternak MM, Golusiński P. miRNAs as Biomarkers for Diagnosing and Predicting Survival of Head and Neck Squamous Cell Carcinoma Patients. *Cancers (Basel)*. 2021 Aug 6; 13 (16): 3980. doi: 10.3390/cancers13163980. PMid:34439138 PMCid:PMC8392400
9. Guo P. The emerging field of RNA nanotechnology. *Nat Nanotechnol*. 2010 Dec; 5 (12): 833-42. doi: 10.1038/nnano.2010.231. PMid:21102465 PMCid:PMC3149862
10. Li H *et al* and Haque F, Liang XJ, Guo P. RNA as a stable polymer to build controllable and defined nanostructures for material and biomedical applications. *Nano Today.* 2015 Oct 1; 10 (5): 631-655. doi: 10.1016/j.nantod.2015.09.003. PMid:26770259 PMCid:PMC4707685
11. Xiao D *et al* and Chen P, Wang Y, Zhang L. Targeted delivery of cancer drug paclitaxel to chordomas tumor cells via an RNA nanoparticle harboring an EGFR aptamer. *Colloids Surf B Biointerfaces*. 2022 Apr; 212: 112366. doi: 10.1016/j.colsurfb.2022.112366. PMid:35144131
12. Liu J *et al* and Chen C, Shen G, Guo P. Fabrication of stable and RNase-resistant RNA nanoparticles active in gearing the nanomotors for viral DNA packaging. *ACS Nano*. 2011 Jan 25; 5 (1): 237-46. doi: 10.1021/nn1024658. PMid:21155596 PMCid:PMC3026857
13. Rychahou P *et al* and Valentino J, Guo P, Evers BM. Delivery of RNA nanoparticles into colorectal cancer metastases following systemic administration. *ACS Nano*. 2015 Feb 24; 9 (2): 1108-16. doi: 10.1021/acsnano.5b00067. PMid:25652125 PMCid:PMC4613746
14. Lee TJ *et al* and Kaur B, Guo P, Croce CM. RNA nanoparticle as a vector for targeted siRNA delivery into glioblastoma mouse model. *Oncotarget*. 2015 Jun 20; 6 (17): 14766-76. doi: 10.18632/oncotarget.3632. PMid:25885522 PMCid:PMC4558114
15. Binzel DW *et al* and Shu D, Guo B, Guo P. Specific Delivery of MiRNA for High Efficient Inhibition of Prostate Cancer by RNA Nanotechnology. *Mol Ther*. 2016 Aug; 24 (7): 1267-77. doi: 10.1038/mt.2016.85. Epub 2016 Apr 29. Erratum in: Mol Ther. 2024 Jul 19: S1525-0016(24)00465-9. doi: 10.1016/j.ymthe.2024.07.010.
16. Zhang Y *et al* and Shu D, Guo P, Zhang X. Overcoming Tamoxifen Resistance of Human Breast Cancer by Targeted Gene Silencing Using Multifunctional pRNA Nanoparticles. *ACS Nano*. 2017 Jan 24; 11 (1): 335-346. doi: 10.1021/

acsnano.6b05910. PMid:27966906 PMCid:PMC5488869
17. Cui D *et al* and Li H, Brand-Saberi B, Guo P. Regression of Gastric Cancer by Systemic Injection of RNA Nanoparticles Carrying both Ligand and siRNA. *Sci Rep*. 2015 Jul 3; 5: 10726. doi: 10.1038/srep10726. PMid:26137913 PMCid:PMC4490273
18. Guo S *et al* and Dong Y, Chiu W, Guo P. Ultra-thermostable RNA nanoparticles for solubilizing and high-yield loading of paclitaxel for breast cancer therapy. *Nat Commun*. 2020 Feb 20; 11 (1): 972. doi: 10.1038/s41467-020-14780-5. PMid:32080195 PMCid:PMC7033104
19. Zou Y *et al* and Wang L, Song Z, You F. Analyses of mRNA-seq and miRNA-seq of the brain reveal the sex differences of gene expression and regulation before and during gonadal differentiation in 17β-estradiol or 17α-methyltestosterone-induced olive flounder (Paralichthys olivaceus). *Mol Reprod Dev*. 2020 Jan; 87 (1): 78-90. doi: 10.1002/mrd.23303. PMid:31788912
20. Liu M *et al* and Yang Y, Huang J, Zhang S. Exosomal hsa-miR-21-5p is a biomarker for breast cancer diagnosis. *PeerJ*. 2021 Sep 17; 9: e12147. doi: 10.7717/peerj.12147. PMid:34616615 PMCid:PMC8451442
21. Min J *et al* and Yao CX, Lei G, Xiang YK. Prediction and Analysis of Hepatocellular Carcinoma Related Genes Using Gene Ontology and KEGG. Current Bioinformatics, 2015; 10 (1): 31-38. DOI:10.2174/1574893610011503091314 53.
22. Wu D *et al* and Chen W, Qin N, Zheng Y. Identification of a Prognostic Pyroptostic-Related Model for Head and Neck Squamous Cell Carcinoma Based on LASSO-Cox Regression Analysis. *J Oncol*. 2022 Nov 22; 2022: 1434565. doi: 10.1155/2022/1434565. PMid:36457716 PMCid:PMC9708347
23. Eldosoky MA *et al* and Zaky S, Hamdy NM, Lambert C. Diagnostic Significance of hsa-miR-21-5p, hsa-miR-192-5p, hsa-miR-155-5p, hsa-miR-199a-5p Panel and Ratios in Hepatocellular Carcinoma on Top of Liver Cirrhosis in HCV-Infected Patients. *Int J Mol Sci*. 2023 Feb 5; 24 (4): 3157. doi: 10.3390/ijms24043157. PMid:36834570 PMCid:PMC9962339
24. Pan W, Huang W, Zheng J, Meng Z, Pan X. Construction of a prognosis model of head and neck squamous cell carcinoma pyroptosis and an analysis of immuno-phenotyping based on bioinformatics. *Transl Cancer Res*. 2024 Jan 31; 13 (1): 299-316. doi: 10.21037/tcr-23-922. PMid:38410218 PMCid:PMC10894328
25. Ruffin AT *et al* and Zandberg DP, Ferris RL, Bruno TC. Improving head and neck cancer therapies by immunomodulation of the tumour microenvironment. *Nat Rev Cancer*. 2023 Mar; 23 (3): 173-188. doi: 10.1038/s41568-022-00531-9. PMid:36456755 PMCid:PMC9992112
26. Pashirova TN, Shaihutdinova ZM, Souto EB, Masson P, Mironov VF. Nanoparticle Concentration as an Important Parameter for Characterization of Dispersion and Its Applications in Biomedicine. *Colloid Journal*. 2023; 85 (5): 770-781. https://doi.org/10.1134/S1061933X23600720
27. Xu S *et al* and Liu J, Dong A, Deng L. Sustained release of PTX-incorporated nanoparticles synergized by burst release of DOX·HCl from thermosensitive modified PEG/PCL hydrogel to improve anti-tumor efficiency. *Eur J Pharm Sci*. 2014 Oct 1; 62: 267-73. doi: 10.1016/j.ejps.2014.06.002. PMid:24931190
28. Kwon S *et al* and Hopf Jannasch AS, Ratliff TL, Yeo Y. Systemic Delivery of Paclitaxel by Find-Me Nanoparticles Activates Antitumor Immunity and Eliminates Tumors. *ACS Nano*. 2024 Jan 30; 18 (4): 3681-3698. doi: 10.1021/acsnano.3c11445. PMid:38227965 PMCid:PMC11025439
29. Lee JW *et al* and Lee JY, Yoo NJ, Lee SH. Somatic mutations of EGFR gene in squamous cell carcinoma of the head and neck. *Clin Cancer Res*. 2005 Apr 15; 11 (8): 2879-82. doi: 10.1158/1078-0432.CCR-04-2029. PMid:15837736
30. Alorabi M, Shonka NA, Ganti AK. EGFR monoclonal antibodies in locally advanced head and neck squamous cell carcinoma: What is their current role? *Crit Rev Oncol Hematol*. 2016 Mar; 99: 170-9. doi: 10.1016/j.critrevonc.2015.12.006. PMid:26797287